14th EAWE PhD Seminar on Wind Energy
18-20 September 2018
Vrije Universiteit Brussel, Belgium

An unsteady actuator annulus relationship for simplified multi-kite systems

R Leuthold[a], S Gros[b], and M Diehl[a]

[a]University of Freiburg, Germany
[b]Chalmers University, Sweden

E-mail: rachel.colette.leuthold@imtek.uni-freiburg.de

Abstract

For classical horizontal axis wind turbines, there are many available 'engineering models' that describe the relationship between unsteady induction factors and the nondimensional parameters describing the turbine's performance, such as thrust coefficient. There is, as of yet, no such simple unsteady actuator annulus relationship suitable for multiple-kite airborne wind energy systems (MAWES). This work approximates such a relationship from the Biot-Savart integral of a frozen, periodic vortex tube representing the geometry of a simplified pumping-cycle MAWES. A comparison is made between the behavior of a MAWES as predicted with this new actuator annulus relationship and with the classic Pitt-Peters model.

Keywords: airborne wind energy, multi-kite systems, unsteady induction, vortex tube

1 Introduction

Multi-kite airborne wind energy systems (MAWES) connect two or more equivalent kites via secondary tethers to a main tether. As the kites orbit around the main tether, the MAWES can produce power as the main tether reels-in and out, turning a generator. MAWES induction models may[1] need to include unsteady effects in order to give reasonable results. To the authors' knowledge, no unsteady induction model has yet been developed for such geometries. It is uncertain whether the many existing rotor-specific engineering models[2][3][4][5][6] would be appropriate for MAWES because rotor and MAWES geometry have some key differences:

- *reel-out* The MAWES moves with the freestream during reel-out, and against it during reel-in. This leads to a low apparent velocity during reel-out and a high one during reel-in. As such, the wake's helical vortex system will be periodically scrunched, as would occur during large periodic jumps in a rotor's tip-speed-ratio.
- *radial expansion* The efficiency of a MAWES increases by increasing the kites' flight radius during reel-in. This means that the helical vortex system is not wrapped around a cylindrical body, but a tube (body-of-rotation) with periodically increasing and decreasing radius.
- *elevation angle* The elevation angle is the angle between the main tether and the horizontal, allowing the MAWES to fly at high altitudes. Due to reel-out along the elevation angle, the wake will be shed from a periodically changing altitude. Then, the vortex system centerline will meander up and down, rather than laying linearly.

This paper proposes an engineering model to predict the unsteady, axisymmetric induction experienced by the MAWES; the asymmetric effects of the elevation angle are resigned to future work. The development of such a model occurs in multiple steps: the MAWES geometry is simplified with a number of assumptions (Section 2) to allow the Biot-Savart integral to be evaluated and approximated (Section 3). The resulting model predicts induction behavior (Section 4), leading to some conclusions (Section 5).

2 Assumptions

After simplifying the MAWES geometry, we will make some assumptions typical for the derivation of engineering induction models, and some atypical assumptions that reduce the wake complexity.

Geometric assumptions To focus on axisymmetric effects, we assume that the axis of kite rotation, the main tether, and the dominant wind direction are parallel. Under a uniform freestream wind u_∞ and uniform kite loading among the K kites, only the radial $\hat{\boldsymbol{r}}$ and downwind $\hat{\boldsymbol{x}}$ coordinates remain. These coordinates move in time to be centered at the midpoint of the kites. A sketch of the geometry in these coordinates is given in Figure 1.

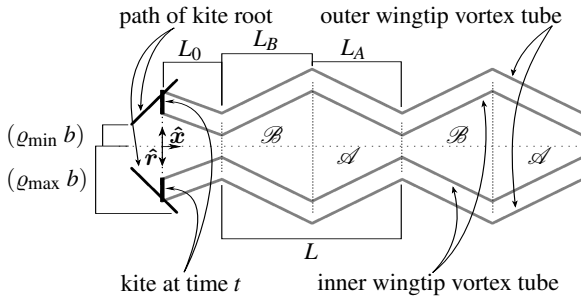

Figure 1: A sketch of MAWES and wake geometry in $\hat{\boldsymbol{r}}, \hat{\boldsymbol{x}}$ plane, during reel-out phase $t \in (0, \tau]$.

One full pumping-cycle is one reel-out phase and one reel-in phase, with total period T. The nondimensional parameter τ is the ratio between the reeling-out time and the total period. The nondimensional time is $t \in (0, 1]$, such that the dimensional time is tT, in seconds.

Let's define the reel-out factor f as the ratio between the tether extension speed and the freestream wind speed. Then, we assume that there is a constant reel-out factor (f_A) during reel-out and a constant reel-in factor (f_B) during reel-in. For periodic orbits, the downstream distance reeled-out must be reclaimed during reel-in: $f_B = -f_A \frac{\tau}{1-\tau}$.

We will assume that the flight radius expands linearly during reel-out, and contracts linearly during reel-in. Then, the maximum radius occurs at maximum tether extension; the minimum radius, at maximum tether retraction. The radial position of the kite's center of gravity is defined as $\varrho\, b$, where ϱ is the relative flight-path radius at any instant, and b is the kite span. The kite is assumed to travel with its spanwise direction along $\hat{\boldsymbol{r}}$ such that the kite's outer and inner wingtips, respectively, have radial locations $(\varrho + \frac{1}{2})b$ and $(\varrho - \frac{1}{2})b$.

We can define a nondimensional parameter ($\beta := \frac{u_\infty T}{b}$) that describes the relative distance by which one fluid element is convected over the course of the period. We also define a nondimensional relative convection distance Λ describing the ratio between a convection distance and the radial position of the kites' outer wingtips. Then, the vorticity shed during one reel-out phase and one reel-in phase is convected, respectively, over distances L_A and L_B, with associated relative convection distances Λ_A and Λ_B:

$$L_A = b\beta(1-f_A)\tau, \quad L_B = b\beta\left(1-\left(1-f_A\right)\tau\right), \quad L = L_A + L_B = b\beta, \quad \Lambda_A = \frac{\beta(1-f_A)\tau}{\frac{1}{2}+\varrho_{\max}}, \quad \Lambda_B = \frac{\beta(1-(1-f_A)\tau)}{\frac{1}{2}+\varrho_{\max}}. \tag{1}$$

To focus our attention on the impact of reel-out, the angular velocity is assumed constant: $\Omega = \frac{2\pi W}{T}$. Here, W is the winding number of the MAWES trajectory. The pitch of the resulting vortex helix system is assumed to be independent of the helix's radius, with a constant value during reel-out (h_A) and another during reel-in (h_B). Similarly, we assume a constant thrust coefficient during reel-out ($C_{\mathrm{T}A}$) and another ($C_{\mathrm{T}B}$) during reel-in.

Typical vortex tube assumptions Assuming a large tip-speed-ratio, the wake behind the MAWES is represented by the summation of frozen vortex tubes. As is frequently done in such models - described well in [2] and [7] - we assume negligible wake expansion (radial induction) and rotation (tangential induction); an equivalent circulation along each kite, which takes one characteristic value during reel-out and another during reel-in; and an infinite number of kites. These assumptions are made for the sake of simplicity, though they represent large approximations to reality.

Due to the linear flight radius expansion and contraction, the vorticity shed from the kites' outer wingtips will form a tube of stacked conic-section segments. The vorticity shed from the inner wingtips will give a similar

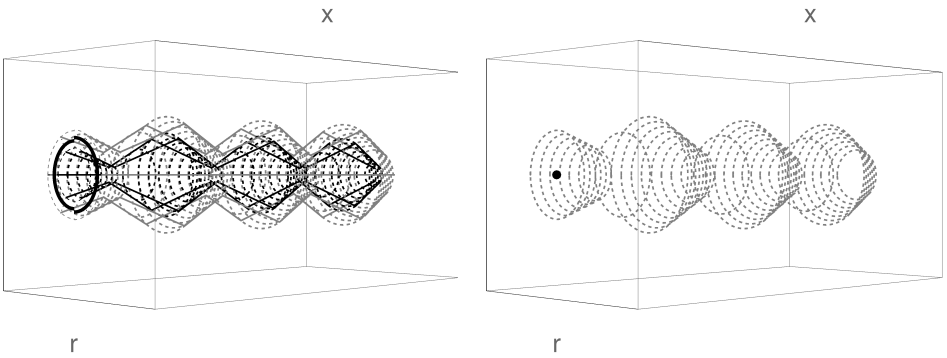

(a) The full wake

(b) The reduced wake: inner wingtip, radial, and longitudinal vortex surfaces removed; observation point shifted to axis

Figure 2: A sketch of the MAWES frozen-wake vortex tubes. Legend: observation path/point (bold), longitudinal vortex tube (solid), tangential vortex tube (dashed), radial vortex annulus (dotted), for outer wingtip (gray), and inner wingtip (black). Vortex surfaces are continuous: spacing indicates local intensity.

conic-section tube with a smaller radius. Naturally, the path followed by the kite root (mid-span) will be between the outer tube and the inner tube. As this engineering model would likely be used for optimization or control, we concern ourselves exclusively with the induction as observed at the kite root, where a Pitot tube would be mounted. This wake geometry is sketched in Figure 2a.

Having neglected radial and tangential induction, the model should only be used to predict axial induction. Due to symmetry and cross-product arguments, neither the radial- nor longitudinal-components of vorticity will create axial-direction induction. Consequently, only the tangential components of vorticity will be considered.

Assumptions for wake reduction Consider a semi-infinite vortex tube of arbitrary cross-section with constant vortex intensity γ. Now, let's take a cross-sectional slice of the vortex tube. On this slice, it is known[8] that the induced velocity outside of the tube's perimeter will be zero, and the induced velocity inside of the tube's perimeter will be constant. If the conic-sections that make up the wake are long in comparison to their radius ($\Lambda \gg 1$), the outer wingtip vortex tube will contribute significantly more to the induction observed at the kite root than the inner wingtip vortex tube. Since the goal is an engineering model rather than a high-fidelity model, we assume, then, that the vorticity shed by the inner wingtips is negligible.

Furthermore, if the induction is roughly radially-independent within the vortex tube, then the observation point can be moved to any interior radial position. The most convenient observation point is on the axis, as symmetry greatly simplifies the Biot-Savart integral. On the basis of these assumptions, we simplify the full vortex tube structure shown in Figure 2a to the reduced structure shown in Figure 2b.

Next, we will integrate the Biot-Savart induction over this structure, in order to approximate the induction factor.

3 The proposed engineering model

In this section, we will find the Biot-Savart integral for a tangential conic section, use this integral to propose an engineering model, and give an integral to use when assessing the wake-reduction assumptions.

The velocity induced by a tangential conic section of uniform vortex intensity, as observed on the axis The axial-direction velocity induced at an observation point (r,x) by a vortex ring of circulation Γ and radius R is known[7] to be $u_{x\text{ring}}(\Gamma,r,x,R)$. Then, the induced velocity at an observation point on the ring's axis can be found:

$$u_{x\text{ring}}(\Gamma,r,x,R) = \frac{\Gamma}{2\pi}\frac{\left(\frac{R^2-r^2-x^2}{(r-R)^2+x^2}E\left(\frac{4rR}{(r+R)^2+x^2}\right)+K\left(\frac{4rR}{(r+R)^2+x^2}\right)\right)}{\sqrt{(r+R)^2+x^2}} \quad \Rightarrow \quad u_{x\text{ring}}(\Gamma,0,x,R) = \frac{\Gamma}{2}\frac{R^2}{(R^2+x^2)^{3/2}}. \quad (2)$$

Let's form a vortex tube along the axis $\hat{\boldsymbol{x}}$ by stacking rings of contant intensity γ and variable radius $R(s)$ at positions $x(s)$ for $s \in [0,1]$. (The intensity is defined with respect to the circulation: $\Gamma = \int_0^1 \gamma \frac{\mathrm{d}x}{\mathrm{d}s} \mathrm{d}s$.) If the vortex tube is a conic section, it can be described with linear parameterizations $R(s) = R_0 + (R_1 - R_0)s$ and $x(s) = x_0 + (x_1 - x_0)s$. This will give an $\hat{\boldsymbol{x}}$-direction induction at the cylindrical coordinates $(0,0)$ equal to:

$$u_x(\gamma, R_0, R_1, x_0, x_1) = \int_0^1 \frac{\gamma}{2} \frac{R(s)^2 \ \mathrm{d}s}{\left(R(s)^2 + x(s)^2\right)^{3/2}} = \frac{\gamma}{2} \left(\frac{(x_1 - x_0)(R_1 - R_0)^2 \left(\ell_1 - \ell_0\right)}{\left((R_1 - R_0)^2 + (x_1 - x_0)^2\right)^{3/2}} + \frac{(x_1 - x_0)\left(\ell_2 + \ell_3\right)}{\left((R_1 - R_0)^2 + (x_1 - x_0)^2\right)} \right), \quad \text{(3a)}$$

$$\ell_0 = \log\left(\sqrt{\left(R_0^2 + x_0^2\right)\left((R_1 - R_0)^2 + (x_1 - x_0)^2\right)} + R_0(R_1 - R_0) + x_0(x_1 - x_0) \right), \quad \ell_2 = \frac{R_0(R_1 - R_0) + x_0(x_0 - x_1)}{\sqrt{R_0^2 + x_0^2}}, \quad \text{(3b)}$$

$$\ell_1 = \log\left(\sqrt{\left(R_1^2 + x_1^2\right)\left((R_1 - R_0)^2 + (x_1 - x_0)^2\right)} + R_1(R_1 - R_0) + x_1(x_1 - x_0) \right), \quad \ell_3 = \frac{R_1(R_0 - R_1) + x_1(x_1 - x_0)}{\sqrt{R_1^2 + x_1^2}}. \quad \text{(3c)}$$

As a sanity check, (3) gives the known[8] induction from a finite and semi-infinite cylinder on their axes:

$$u_x(\gamma, R, R, x_0, x_1) = \frac{\gamma}{2} \left(\frac{x_1}{\sqrt{R^2 + x_1^2}} - \frac{x_0}{\sqrt{R^2 + x_0^2}} \right), \qquad \lim_{x_1 \to \infty} u_x(\gamma, R, R, 0, x_1) = \frac{\gamma}{2}. \quad (4)$$

Now, we approximate the MAWES induction by assembling the reduced-wake from tangential conic sections.

The engineering model, assembled from a periodic conic-section vortex tube Given the assumed geometry, the wake is represented as a semi-infinite and periodic stack of tangential conic sections. Let's designate conic-sections shed during reel-out and reel-in, respectively, as having types $\mathscr{A}$ and $\mathscr{B}$. Then, the wake of a reeling-out MAWES will consist of one partial conic section of type $\mathscr{A}$, followed by full conic sections of type $\mathscr{B}$, $\mathscr{A}$, $\mathscr{B}$... This order is reversed for a reeling-in MAWES.

For the assumed linearly-expanding radius, type $\mathscr{A}$ conic sections start with radius $R_{\max} = (\varrho_{\max} + \frac{1}{2})b$ and end with radius $R_{\min} = (\varrho_{\min} + \frac{1}{2})b$. Conic sections of type $\mathscr{B}$ start with radius $R_{\min}$ and end with radius $R_{\max}$. The dimensions of the partial conic section - length $L_0(t)$ and initial radius $R_0(t) = (\varrho_0\,(t) + \frac{1}{2})b$ - and the reel-out factor $f(t)$ can be found with:

$$f(t) = \begin{cases} 1 - f_A \\ 1 + \frac{f_A \tau}{1 - \tau} \end{cases} \quad L_0(t) = \begin{cases} b\beta(1 - f_A)t \\ b\beta\left(1 + \frac{f_A \tau}{1 - \tau}\right)(t - \tau) \end{cases} \quad \varrho_0\,(t) = \begin{cases} \varrho_{\min} + \frac{t}{\tau}(\varrho_{\max} - \varrho_{\min}) & \text{for } 0 < t \leq \tau, \\ \varrho_{\max} + \frac{t - \tau}{1 - \tau}(\varrho_{\min} - \varrho_{\max}) & \text{for } \tau < t \leq 1. \end{cases} \quad (5)$$

The pitch with which helical vortices would wrap around a conic section is found with $h = \pi \frac{u(1-f)}{\Omega}(1 + \sqrt{1 - C_{\mathrm{T}}})$ such that vortex tube models are consistent[8] with axial momentum theory. This gives pitches h_A and h_B for sections of type $\mathscr{A}$ and $\mathscr{B}$, respectively, as:

$$h_A = \frac{1}{2} b\beta(1 - f_A)\left(\frac{1 + \sqrt{1 - C_{\mathrm{T}A}}}{W}\right), \quad h_B = \frac{1}{2} b\beta\left(1 + \frac{f_A \tau}{1 - \tau}\right)\left(\frac{1 + \sqrt{1 - C_{\mathrm{T}B}}}{W}\right). \quad (6)$$

The vortex intensities of type $\mathscr{A}$ and $\mathscr{B}$ conic sections - respectively, γ_A and γ_B - are found by distributing the sections' circulations - respectively, Γ_A and Γ_B - over the pitch. That is: $\gamma_A = \frac{\Gamma_A}{h_A}$ and $\gamma_B = \frac{\Gamma_B}{h_B}$. The Kutta-Joukowski expression gives the relationship between the circulation and the thrust coefficient.

$$C_{\mathrm{T}} = \frac{K\rho\Omega r' \Gamma_1 \mathrm{d}r'}{\frac{1}{2}\rho u_\infty^2 (1 - f)^2 (2\pi r' \mathrm{d}r')} = \Gamma \frac{2TW}{b^2\beta^2(1 - f)^2} \Rightarrow \Gamma_A = \frac{b^2}{T} \frac{\beta^2 C_{\mathrm{T}A}(1 - f_A)^2}{2W}, \Gamma_B = \frac{b^2}{T} \frac{\beta^2 C_{\mathrm{T}B}(1 + f_A \frac{\tau}{1 - \tau})^2}{2W}, \quad (7)$$

where Γ_1 is the circulation in one kite and $\Gamma = K\Gamma_1$. As thrust points axially and the tangential induction is negligible, the velocity used in the scalar Kutta-Joukowski expression is the angular velocity.

According to the wake-reduction assumptions, we now approximate the axial-direction induced-velocity at the kite root as $u_{\mathrm{i}}(t)$. This induced velocity is found using the induced velocities during reel-out $u_{\mathrm{i},A}$ and reel-in $u_{\mathrm{i},B}$ and an infinite sum where $M=N=P=Q=\infty$:

$$u_{\mathrm{i}}(t) = \begin{cases} u_{\mathrm{i},A} & \text{for } 0<t\leq\tau, \\ u_{\mathrm{i},B} & \text{for } \tau<t\leq 1, \end{cases} \tag{8a}$$

$$\begin{aligned} u_{\mathrm{i},A} \approx\ & u_x\left(\gamma_A,\, R_0,\, R_{\min},\, 0,\, L_0\right) + \textstyle\sum_{m=1}^{M} u_x\left(\gamma_B,\, R_{\min},\, R_{\max},\, L_0+(m-1)L,\, L_0+(m-1)L+L_B\right)\ldots \\ & + \textstyle\sum_{n=1}^{N} u_x\left(\gamma_A,\, R_{\max},\, R_{\min},\, L_0+(n-1)L+L_B,\, L_0+nL\right), \end{aligned} \tag{8b}$$

$$\begin{aligned} u_{\mathrm{i},B} \approx\ & u_x\left(\gamma_B,\, R_0,\, R_{\max},\, 0,\, L_0\right) + \textstyle\sum_{p=1}^{P} u_x\left(\gamma_A,\, R_{\max},\, R_{\min},\, L_0+(p-1)L,\, L_0+(p-1)L+L_A\right)\ldots \\ & + \textstyle\sum_{q=1}^{Q} u_x\left(\gamma_B,\, R_{\min},\, R_{\max},\, L_0+(q-1)L+L_A,\, L_0+qL\right). \end{aligned} \tag{8c}$$

Finally, we normalize the induced velocity using the definition of the induction factor $a(t) := \frac{u_{\mathrm{i}}(t)}{u_\infty(1-f(t))}$.

One logical method of approximating an infinite sum is truncation. If the relative convection lengths Λ_A and Λ_B are much greater than 1, it is likely that only the first partial conic section and the first full conic section are already responsible for the majority of the induction. In this case, we might set $M=P=1$ and $N=Q=0$.

The numerical integral without wake-reduction To assess the impact of the wake-reduction assumptions, we might numerically integrate the Biot-Savart expression for both tangential vortex tubes, as observed at the kite root. We can compute the induction factor from the induced velocity $u_{\mathrm{i,num}}(t)$, using a large number of shed periods S:

$$u_{\mathrm{i,num}}(t) = \int_0^{2S+1} \left(u_{x\mathrm{ring}}\left(\Gamma(s,t),\, \varrho_0(t)b,\, x(s,t),\, R_{\mathrm{out}}(s,t)\right) - u_{x\mathrm{ring}}\left(\Gamma(s,t),\, \varrho_0(t)b,\, x(s,t),\, R_{\mathrm{in}}(s)\right)\right) \mathrm{d}s. \tag{9}$$

Here, $R_{\mathrm{out}}(s,t)$ is the radius of the outer wingtip's vortex tube found by applying $R_{\min}=(\varrho_{\min}+\frac{1}{2})b$ and $R_{\max}=(\varrho_{\max}+\frac{1}{2})b$ to (10). Similarly, $R_{\mathrm{in}}(s,t)$ is the radius of the inner wingtip's vortex tube, found by applying $R_{\min}=(\varrho_{\min}-\frac{1}{2})b$ and $R_{\max}=(\varrho_{\max}-\frac{1}{2})b$ to (10), with step function $U(\cdot)$:

$$R(s,t) = \begin{cases} \left(R_0+(R_{\min}-R_0)s\right)\mathrm{U}\left((s)(1-s)\right) + \textstyle\sum_{n=1}^{S}\left(R_{\min}+(R_{\max}-R_{\min})(s-2n+1)\right)\mathrm{U}\left((s-2n+1)(2n-s)\right)\ldots \\ \quad + \textstyle\sum_{n=1}^{S}\left(R_{\max}+(R_{\min}-R_{\max})(s-2n)\right)\mathrm{U}\left((s-2n)(2n+1-s)\right) & \text{for } 0<t\leq\tau, \\ \left(R_0+(R_{\max}-R_0)s\right)\mathrm{U}\left((s)(1-s)\right) + \textstyle\sum_{n=1}^{S}\left(R_{\max}+(R_{\min}-R_{\max})(s-2n+1)\right)\mathrm{U}\left((s-2n+1)(2n-s)\right)\ldots \\ \quad + \textstyle\sum_{n=1}^{S}\left(R_{\min}+(R_{\max}-R_{\min})(s-2n)\right)\mathrm{U}\left((s-2n)(2n+1-s)\right) & \text{for } \tau<t\leq 1. \end{cases} \tag{10}$$

The starting radius R_0 is found as $(\varrho_0+\frac{1}{2})b$ for the outer vortex tube, and $(\varrho_0-\frac{1}{2})b$ for the inner vortex tube, with ϱ_0 given by (8a). Then, the parameterized axial position $x(s)$ of the rings and the circulation $\Gamma(s)$ for vortex intensities γ_A and γ_B are:

$$\Gamma = \begin{cases} \gamma_A L_0 \mathrm{U}\left((s)(1-s)\right)\ldots \\ \quad + \textstyle\sum_{n=1}^{S}\gamma_B L_B \mathrm{U}\left((s-2n+1)(2n-s)\right)\ldots \\ \quad + \textstyle\sum_{n=1}^{S}\gamma_A L_A \mathrm{U}\left((s-2n)(2n+1-s)\right), \\ \gamma_B L_0 \mathrm{U}\left((s)(1-s)\right)\ldots \\ \quad + \textstyle\sum_{n=1}^{S}\gamma_A L_A \mathrm{U}\left((s-2n+1)(2n-s)\right)\ldots \\ \quad + \textstyle\sum_{n=1}^{S}\gamma_B L_B \mathrm{U}\left((s-2n)(2n+1-s)\right), \end{cases} \quad x = \begin{cases} L_0 s \mathrm{U}\left((s)(1-s)\right)\ldots & \text{for } 0<t\leq\tau \\ \quad + \textstyle\sum_{n=1}^{S}\left(L_0+(n-1)L+L_B(s-2n+1)\right)\mathrm{U}\left((s-2n+1)(2n-s)\right)\ldots & \\ \quad + \textstyle\sum_{n=1}^{S}\left(L_0+(n-1)L+L_B+L_A(s-2n)\right)\mathrm{U}\left((s-2n)(2n+1-s)\right), & \\ L_0 s \mathrm{U}\left((s)(1-s)\right)\ldots & \text{for } \tau<t\leq 1 \\ \quad + \textstyle\sum_{n=1}^{S}\left(L_0+(n-1)L+L_A(s-2n+1)\right)\mathrm{U}\left((s-2n+1)(2n-s)\right)\ldots & \\ \quad + \textstyle\sum_{n=1}^{S}\left(L_0+(n-1)L+L_A+L_B(s-2n)\right)\mathrm{U}\left((s-2n)(2n+1-s)\right). & \end{cases} \tag{11}$$

Though the integral (9) is not an exact solution, due to the multiple strong underlying assumptions given in section 2, it is closer to a physical solution than the engineering model. Consequently, this numerical integral can be used to consider the impact of wake-reduction on the proposed engineering model.

4 Trends in the induction behavior

Using certain relevant test cases and computation models, we will compare the trends in the induction behavior.

The test cases and methods under comparison The induction behavior will be considered for a selection of 7 relevant test-cases - for illustrative combinations of typical horizontal axis wind turbine (HAWT) or MAWES parameters - as defined in Table 1a. These test-cases are scaled by values associated with the Ampyx AP2 kite[1] ($b = 5.5$m and $T = 45$s), with some nondimensional parameters fixed ($\beta = 98$, $C_{TA} = 8/9$, $W = 5$, and $\tau = 3/4$) to give a more even comparison.

Table 1: Test case parameters and computation times

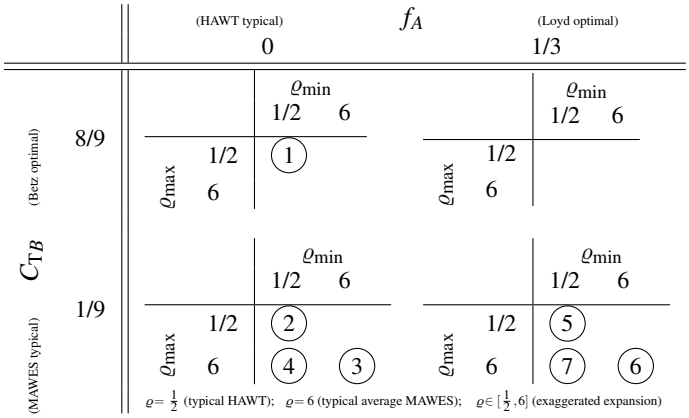

(a) Index numbers (circled) of test cases, assigning parameters

model	wall-time [s]	scaled [-]
Steady	$2.7 \cdot 10^{-6}$	1
Pitt/Peters	$2.4 \cdot 10^{-2}$	$8.9 \cdot 10^{3}$
Integration	$2.8 \cdot 10^{-1}$	$1.1 \cdot 10^{5}$
Engineering	$4.0 \cdot 10^{-4}$	$1.5 \cdot 10^{2}$

(b) Approximate average dimensional and scaled wall-times per model, when solved in `Mathematica` on a personal computer.

We compare the induction behavior predicted by four models. For each model, we plot $a(t)$ vs t over the selected test cases (Figure 3). Further, we record the average computation times for $a(t)$ (Table 1b). The four models are:

- *Steady* the steady axial momentum theory with $a = \frac{1}{2}(1 - \sqrt{1 - C_T})$.
- *Pitt/Peters* the corrected axisymmetric Pitt/Peters model [9] such that $\frac{16}{3\pi}\dot{a} + 4a(1-a) = C_T$, using the derivative $\dot{a} = \frac{1}{T}\frac{da}{dt}$ and the initial condition of $a(0) = \frac{1}{2}(1 - \sqrt{1 - C_{TB}})$.
- *Integration* the numerical integration of (9) including both wingtips' tangential vortex tubes, as observed at the kite's radial location, with $S = 10$.
- *Engineering* the engineering approximation given by (8) with $M = P = 1$ and $N = Q = 0$.

As none of these low-order models is a valid verification model, the goal is to determine whether the models are able to represent reel-out and radial expansion in a reasonable manner. This behavior is described below.

The steady HAWT case: case 1 The four models predict the same behavior: a steady-state value of $\frac{1}{3}$.

The unsteady HAWT case: case 2 The four models show the same steady-state values. Here, the numerical integral model (and it's overlapping engineering model) predict a slightly faster response time than the Pitt/Peters model. Further study would be needed to see how the response time predicted by the numerical integral depends on those assumptions typically made for frozen-wake vortex tubes without wake expansion.

The case with large flight radius and a C_T jump: case 3 The predicted steady-state values are again equal for all models though the engineering model responds slower at a larger radius than the numerical integration model. This suggests that for increasing radius, the wake-reduction approximations become less accurate as ϱ increases. This is because Λ will decrease as $\varrho_{\max}$ increases, and the wake-reduction assumptions relied on large Λ values.

The case with radial expansion and a C_T jump: case 4 With radial expansion, the steady state values of the numerical integral are offset from those of the steady and Pitt/Peters model. This offset is a slight decrease during reel-out ($t \in (0, \tau]$), and a slight increase during reel-in ($t \in (\tau, 1]$). This offset appears reasonable, as the tube diameter at the kite's $\hat{x}$ position is increasing during reel-out and decreasing during reel-in. From (2) we know that a vortex ring of equivalent circulation will induce less velocity as its radius increases. The engineering model exaggerates the offsets predicted by the numerical model. On another note, when ϱ takes the value it had in case 2 (at $t = 0$), the engineering model's response speed is the same as in case 2; when ϱ takes the case 3 value (at $t = \tau$), the case 3 response speed is seen.

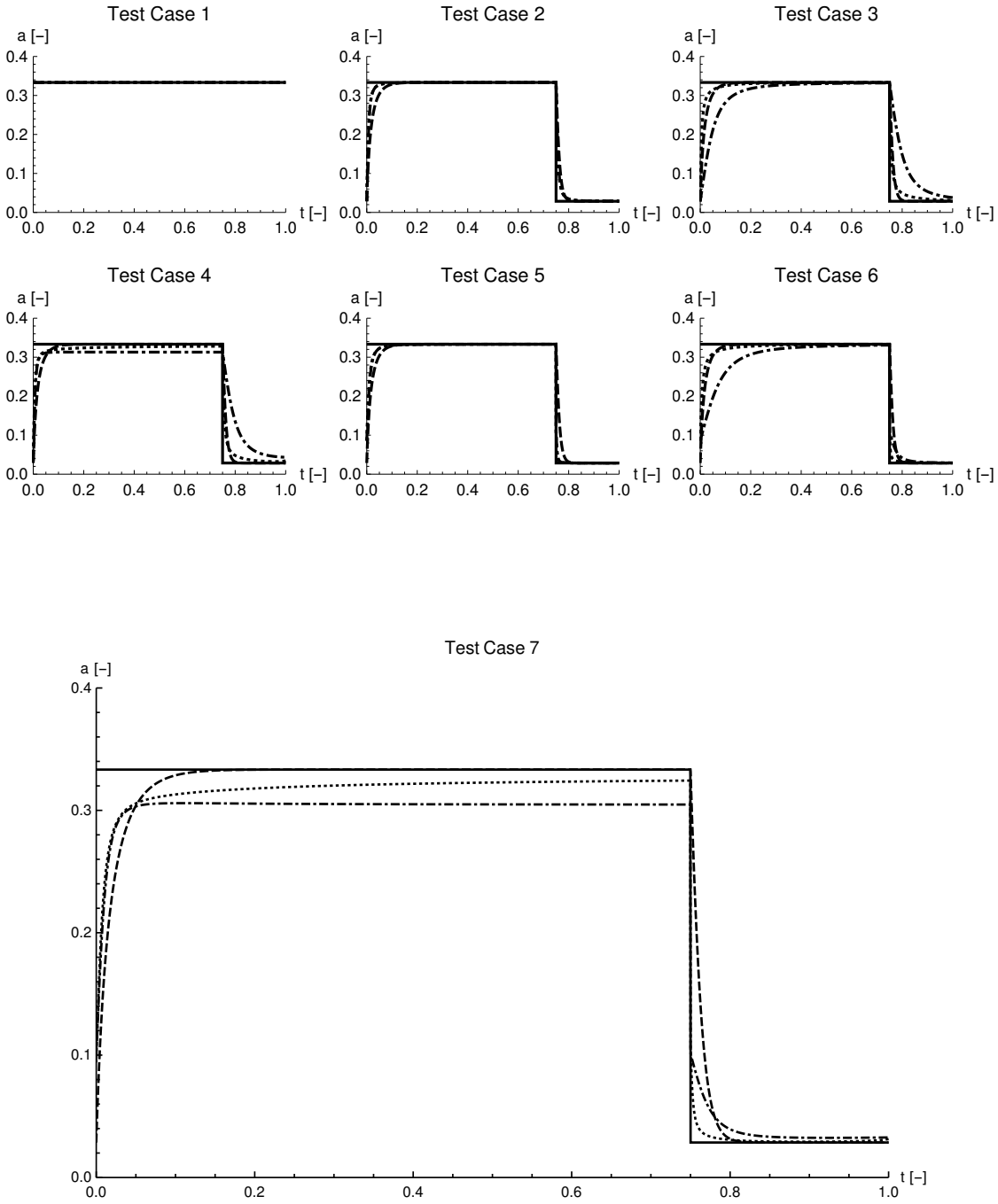

Figure 3: Induction factors compared to time for selected test cases. The legend is as follows: steady model (solid); Pitt/Peters model (dashed); numerical integration model (dotted); and proposed engineering model (dash-dotted).

The cases with reel-out and a C_T jump: cases 5 and 6 The behaviors in cases 5 and 6 shows similar trends to those in cases 2 and 3. The response times during reel-out and reel-in are, respectively, stretched and condensed, as the apparent wind is slower during reel-in and faster during reel-out. That is, the apparent wind-speed effectively re-scales the behavior with respect to time. Due to this re-scaling effect, the reel-in predictions of the numerical integral and the engineering model are much closer together in case 6 than in case 3.

The MAWES case: case 7 This case shows the combined behaviors of the previous test cases. With respect to steady-state values: the engineering model exaggerates the offsets predicted by the numerical integral from the steady and rotor-derived Pitt/Peters model. During reel-out, the response time of the engineering model is approximately that of the numerical model; in reel-in, the engineering model is slow in comparison to the numerical model. After including the effects of reel-out and radial-expansion, the response speed of all three unsteady models are comparable.

Based on the trends described for the above test cases, we now summarize some conclusions.

5 Conclusion

This paper proposes an engineering model to predict the unsteady induction over the MAWES actuator annulus. This engineering model demonstrates certain changes to the steady-state induction behavior of a simplified axisymmetric MAWES undergoing radial expansion and contraction, that cannot be predicted with either steady or rotor-specific unsteady models. The reasonable qualitative behavior - and fast computation time - of the engineering model suggest that it may be useful where the influence of reel-out and/or radial expansion must be considered, but fast computation time is more important than perfect accuracy.

Subject to verification and validation, this engineering model appears to be a first step towards a fast, unsteady induction model suitable to MAWES geometry and operating strategies. In addition to validation, future work should expand the unsteady induction model to include the asymmetric effects relevant to MAWES: nonzero elevation angle, tilt angle, and nonuniform thrust per kite.

Acknowledgements

Thank you to Christoph Sieg for helpful discussions and encouragement. Additionally, this research was supported by the EU via H2020-ITN-AWESCO (642 682), by the Federal Ministry for Economic Affairs and Energy (BMWi) via eco4wind (0324125B) and DyConPV (0324166B), and by DFG via Research Unit FOR 2401.

References

[1] Leuthold R, De Schutter J, Malz E, Licitra G, Gros S and Diehl M 2018 European Control Conference (Limassol, Cyprus)

[2] Coleman R P, Feingold A M and Stempin C W 1945 Evaluation of the induced-velocity field of an idealized helicopter rotor. Tech. rep. NACA ARR-L5E10 Langley Field, Virgina, USA

[3] Pitt D and Peters D 1981 Vertica **5** 21–34

[4] Øye S 1990 3rd IEA Symposium on the Aero-Dynamics of Wind Turbines (Harwell, UK)

[5] Snel H and Schepers J G 1991 European Wind Energy Conference (Amsterdam, the Netherlands)

[6] Yu W, Ferreira C S, van Kuik G A M and Schepers G Wind Energy Under Review

[7] Branlard E and Gaunaa M 2015 Wind Energy **18** 1973–1987 ISSN 10954244

[8] Branlard E 2017 Wind turbine aerodynamics and vorticity-based methods : fundamentals and recent applications (Roskilde, Denmark: Springer) ISBN 9783319551630

[9] Burton T, Sharpe D, Jenkins N and Bossanyi E 2011 Wind energy handbook (Chichester, West Sussex, England: Wiley) ISBN 9780470699751